CONDITIONS OF FORMATION OF LIZARDITE, CHRYSOTILE AND ANTIGORITE, CASSIAR, BRITISH COLUMBIA

DAVID S. O'HANLEY[1] AND FREDERICK J. WICKS

Department of Mineralogy, Royal Ontario Museum, Toronto, Ontario M5S 2C6

ABSTRACT

Observations at the Cassiar (British Columbia) chrysotile asbestos deposit have defined a continuous series of serpentine textures, between pseudomorphic and nonpseudomorphic. These minerals and textures are distributed with respect to shear zones in the interior of the serpentinite such that the degree of recrystallization and replacement increases as the shear zones are approached. Patterns of spatial distribution suggest that recrystallization and replacement were caused by infiltration-driven metamorphism as the serpentinite equilibrated with an externally derived fluid. The shear zones served as conduits for the fluid. The recrystallization and replacement of lizardite formed after olivine and of that formed after enstatite proceed independently early in the process, such that composition of the various serpentine minerals was controlled by the bulk composition of the precursor. Later in the process, Fe^{2+}/Mg, Cr/Al and $Fe^{3+}/(Mg + Si)$ values, and the distribution of boron, between serpentine after olivine and that formed after enstatite indicate that equilibrium was closely approached. The formation of a chrysotile + antigorite assemblage marks this transition. The recrystallization of lizardite and its replacement by chrysotile + antigorite occurred at $250 \pm 25°C$ and a $P(H_2O)$ of less than 1 kbar. The temperatures and pressures of serpentinization can be modeled in the system $MgO–SiO_2–H_2O$ (MSH) because: 1) clinochlore is stabilized by the breakdown of chromite, rather than a serpentine mineral, and 2) magnetite is both a product and a reactant in the conversion of lizardite to antigorite, indicating that it is not an essential compound in the conversion of lizardite to antigorite. The mineralogy, textures and compositions of lizardite and chrysotile indicate that they are polymorphs in the MSH system.

Keywords: serpentinite, serpentine, recrystallization, replacement, infiltration metamorphism, mineral stability, Cassiar, British Columbia.

SOMMAIRE

Notre étude du gisement d'amiante à chrysotile de Cassiar, en Colombie-Britannique, a permis de définir une série continue de textures, allant de pseudomorphique à non pseudomorphique, impliquant les minéraux du groupe de la serpentine. Les minéraux et les textures sont répartis par rapport à des zones de cisaillement dans la partie interne du massif de serpentinite de façon telle que le degré de recristallisation et de remplacement augmente vers ces zones. En gros, cette répartition témoignerait d'un métamorphisme dû à l'infiltration d'une phase fluide externe hors d'équilibre avec la serpentinite. Les zones de cisaillement ont servi de conduits. La recristallisation et le remplacement de la lizardite formée aux dépens de l'olivine et de celle formée aux dépens de l'enstatite ont d'abord progressé indépendamment, de telle sorte que la composition des diverses formes de serpentine étaient régies par la composition du minéral précurseur. Plus tard, les rapports Fe^{2+}/Mg, Cr/Al et $Fe^{3+}/(Mg + Si)$ et la distribution du bore entre la serpentine qui remplace l'olivine et celle qui remplace l'enstatite indiquent que l'équilibre était atteint à plus large échelle. La formation d'un assemblage à chrysotile + antigorite marque cette transition. La recristallisation de la lizardite et son remplacement par chrysotile + antigorite ont eu lieu à environ $250 \pm 25°C$ et à une valeur de $P(H_2O)$ inférieure à 1 kbar. Nous nous servons du système $MgO–SiO_2–H_2O$ (MSH) comme schéma pour reconstituer la température et la pression de la serpentinisation, parce que 1) le clinochlore est stabilisé par la décomposition de la chromite, plutôt qu'une serpentine, 2) la magnétite est soit un produit ou un réactif dans la conversion de la lizardite à l'antigorite, indication qu'elle n'est pas essentielle dans la conversion de la lizardite à l'antigorite. D'après la minéralogie, les textures et les compositions de la lizardite et la chrysotile, celles-ci seraient en fait des polymorphes dans le système MSH.

(Traduit par la Rédaction)

Mots-clés: serpentinite, serpentine, recristallisation, remplacement, métamorphisme par infiltration, stabilité des minéraux, Cassiar, Colombie-Britannique.

[1] Present address: Trinity School at River Ridge, 2300 East 88th Street, Bloomington, Minnesota 55425-2187, U.S.A.

INTRODUCTION

The phase relations amongst the serpentine minerals lizardite, chrysotile, and antigorite have puzzled researchers since the three minerals were recognized and defined by Whittaker & Zussman (1956). Some investigators of antigorite-dominated metamorphic terranes have interpreted the phase relations only in terms of antigorite and chrysotile (Evans *et al.* 1976) and have left out lizardite, the most commonly occurring of the three minerals. Others have modeled the phase relationships in terms of lizardite and antigorite (Caruso & Chernosky 1979) and have left out chrysotile. Recently, O'Hanley (1987) and O'Hanley *et al.* (1989a) have employed chemographic analysis using dual networks to develop possible solutions to the serpentine phase-relations problem, using all three serpentine minerals and other relevant phases.

Deposits of chrysotile asbestos in serpentinized peridotites contain a variety of textures made up of various combinations of the serpentine minerals lizardite, chrysotile, and antigorite (Wicks & Whittaker 1977). Thus, they form a natural laboratory in which to study the phase-relations problem. The Cassiar serpentinite, in north-central British Columbia, is an ideal body for this type of study. It contains all the complexities and variations of chrysotile asbestos deposits, but it is small enough to map in detail in a reasonable period of time. The mine was in production during the period of the research project (1987–1988), and the company, Cassiar Mining Corporation, provided access to the mining records. This meant that the rock already mined could be included in the analysis, making our study more complete.

The variety of serpentine textures in asbestos deposits creates two initial impressions: first, the serpentine minerals and textures seem to be randomly distributed with respect to geological structure, and second, that serpentinization is a disequilibrium process in which local equilibrium cannot be applied. However, this is not the case. The textures and minerals are systematically distributed with respect to the geological structure, and record the geological processes that produced them. The minerals also reflect not only local equilibrium, but equilibrium at a larger scale, for example, between lizardite after olivine and lizardite after enstatite (referred to as "bastite"). Thus, it is possible to define zones consisting of distinct assemblages of serpentine minerals [called "isoregimes" by Laurent (1980)], upon which petrological interpretations can be based.

It is the principal goal of this paper to establish the conditions of formation of each of the three serpentine minerals through a detailed analysis of the Cassiar chrysotile asbestos mine. Most of the textures at Cassiar correspond to those described by Wicks & Whittaker (1977), but some undocumented variations have been observed. The detailed mapping of the structure within the Cassiar serpentinite (O'Hanley 1988, 1990) has provided a framework for the establishment of relations among the pseudomorphic textures, the nonpseudomorphic textures (and textures intermediate between the two) after olivine discussed by Wicks & Plant (1979), the distribution of different types of "bastite", and the distribution of lizardite, chrysotile, and antigorite.

GEOLOGICAL SETTING

The site of the former Cassiar chrysotile asbestos mine is located at Cassiar, in north-central British Columbia. The deposit occurs within the Cassiar serpentinite, which is located at the base of the Sylvester allochthon. The geology of the allochthon has been described by Gabrielse (1963), Harms (1986), O'Hanley (1990), and Nelson & Bradford (1993). The geology of the Cassiar mine has been described by Gabrielse (1960), O'Hanley & Wicks (1987) and O'Hanley (1988, 1990). The allochthon is composed of fault-bounded packages of island-arc and oceanic rocks and has been emplaced on top of late Pre-Cambrian to Devonian platform-type sedimentary rocks. Emplacement of the allochthon occurred between late Triassic and early Cretaceous times, but faults within the allochthon were active during the Permian (Harms 1986). The postemplacement history of this part of British Columbia is dominated by the intrusion of granodioritic to granitic plutons, and by dextral transcurrent faults that have dismembered the allochthonous and accreted terranes (Gabrielse 1985).

The Cassiar serpentinite is enclosed by argillite and chert on its footwall, and by argillite and greenstone on its hanging wall (Fig. 1). The serpentinite is dissected by several shear zones, of which the most important are the 45° shear and the 70° shear. The 45° shear dips 70° east, but contains zones of schistose serpentine and talc–magnetite that dip 45° east (hence its name). The 70° shear dips 70° to the northeast.

The ore zone, defined as serpentinite containing more than 3% chrysotile cross-fiber asbestos veins by volume, is located in the center of the serpentinite, structurally above and spatially associated with the 45° and 70° shears (Fig. 1). There are virtually no veins of chrysotile asbestos in the hanging-wall serpentinite, whereas non-ore veins of magnetite-bearing chrysotile asbestos, are found in several areas in the footwall serpentinite, southwest of the ore zone. A model describing the origin of these and other asbestos veins has been proposed by O'Hanley (1988), who identified two episodes of vein formation at Cassiar. This interpretation is based on vein mineralogy, and vein–vein and vein–matrix cross-cutting relationships. The origin of the veins is associated with displacement along the 45° and 70° shear zones (O'Hanley 1988).

Zones of metasomatic alteration between serpentinite and the argillite, chert, and greenstone are present
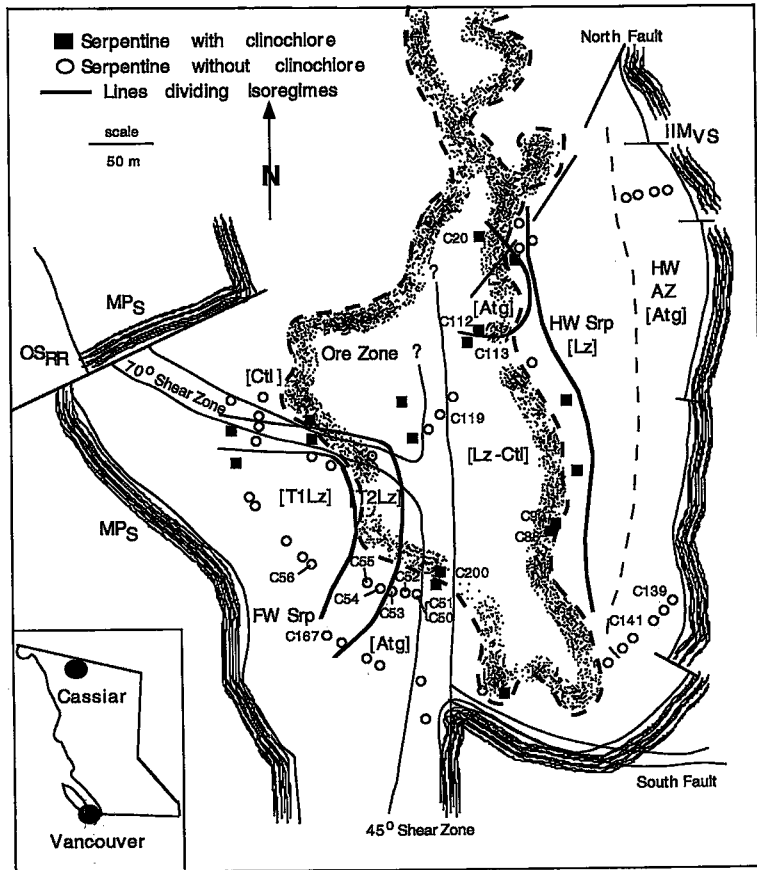
FIG. 1. Geological sketch-map of the Cassiar asbestos mine. The hanging-wall serpentinite (HW Srp) is to the east, and the footwall serpentinite (FW Srp) is to the west of the ore zone. Country rocks consist of Mississippian to Pennsylvanian (MP$_s$) chert and argillite in the footwall, and Mississippian (IIM$_{vs}$) greenstone in the hanging wall. The ore zone, defined by the presence of more than 3% asbestos fiber veins by volume, is in the center of the serpentinite, bounded on the south by the 70° shear and on the west by the 45° shear. Bold lines divide the serpentinite into zones characterized by either specific assemblages of serpentine minerals or specific textures ("isoregimes"). These "isoregimes" include: type-1 lizardite hourglass (T1Lz) and type-2 lizardite hourglass (T2Lz) in the footwall serpentinites, lizardite (Lz) – chrysotile (Ctl) – antigorite (Atg) interlocking textures in and adjacent to the ore zone, lizardite mesh-textures (Lz) in the hanging-wall serpentinite, and antigorite interpenetrating textures (Atg) in the hanging-wall zone of alteration (HW AZ). Samples containing clinochlore are distinguished from those that do not; note there is no relationship between the serpentine "isoregimes" and the distribution of clinochlore. Serpentine "isoregimes" are not coextensive with the ore zone because the ore zone is defined by the presence of chrysotile asbestos veins, not by texture and mineralogy. The hanging-wall zone of alteration (HW AZ) formed through reaction between serpentinite and greenstone; it occurs at the eastern margin of the serpentinite. Sample numbers (*i.e.*, C20, C56, *etc.*) refer to those mentioned either in the text or in the tables.

at both the footwall and the hanging-wall contacts of the serpentinite. The hanging-wall zone of alteration (Fig. 1) is more extensively developed and consists of antigorite formed from lizardite serpentinite, nephrite jade formed from antigorite serpentinite, and quartz, clinozoisite, and minor tremolite after greenstone (Gabrielse 1963, O'Hanley *et al.* 1992). The footwall zone of alteration (not shown on Fig. 1) consists of talc–carbonate ± pyrite after serpentinite; it was not included in this study.

In spite of complete serpentinization, the protolith can be recognized, using the criteria of Wicks (1984), as having been a harzburgite tectonite with proto-granular textures, but both schistosity and kink bands are present in some pseudomorphically serpentinized harzburgite (Wicks & O'Hanley 1988). In hand sample, the serpentinite can be divided into three types based on its color and texture. The ore zone consists of a yellow-green, "glassy" to slightly grainy serpentine with centimeter-sized grains of oxide minerals. The serpentinite between the ore zone and the footwall zone of alteration (FW Srp; Fig. 1) and between the ore zone and the hanging-wall zone of alteration (HW Srp; Fig. 1) consists of a black-veined, green, "glassy" serpentine. The hanging-wall zone of alteration (HW AZ; Fig. 1) consists of a grey-green sugary serpenti-nite.

A minimum age of serpentinization can be estab-lished from geological observations and radiometric dating. East–west-striking normal faults offset textural patterns of the serpentine in both the ore zone and the hanging-wall zone of alteration, indicating that serpentinization predates the normal faults. Several of these normal faults contain undeformed lamprophyre dikes, with ages from 73 to 110 Ma (Nelson & Bradford 1993). These dates indicate that normal faulting, and thus serpentinization, cannot be younger than 73 Ma.

An independent constraint on the minimum age of serpentinization comes from an Ar/Ar cooling age of 94 Ma for a Cr-bearing phlogopite taken from the Road River Group, in the footwall of the Cassiar serpentinite. The rock from which the phlogopite was taken crossed the 300°C isotherm at 94 Ma (Nelson & Bradford 1993). As serpentine recrystallization and replacement at Cassiar occurred at 250 ± 25°C (O'Hanley et al. 1992), recrystallization and replacement must have occurred at or near this time.

Experimental Techniques

The terminology of Mercier & Nicolas (1975) is used for peridotite textures, and that of Wicks & Whittaker (1977), as modified by Wicks & O'Hanley (1988), is used for serpentinite textures. A microbeam X-ray camera was used to identify the minerals *in situ* in thin section, following the procedures of Wicks & Zussman (1975), so that the textures could be related to specific minerals. The X-ray-diffraction experiments utilized Ni-filtered Cu radiation during runs of 8 hours under vacuum. A total of 58 microbeam films were obtained from 16 samples. Whole-rock analyses were obtained from X-Ray Assay Laboratories, Toronto, using X-ray fluorescence spectroscopy. Fused beads were used for major elements, and powder pellets were used for minor elements. H_2O^+, H_2O^- and FeO were determined from wet-chemical methods. Alpha-track mapping was used to determine qualita-

tively the distribution of B in several samples from the Cassiar serpentinite (Carpenter 1972, Higgins et al. 1984).

Mineral compositions were determined by electron microprobe. Analyses were carried out using a JEOL 8600 Superprobe housed at the University of Western Ontario. Operating conditions were 15 kV and 10 nA with a counting time of 20 seconds. Natural minerals were used as standards.

The techniques and results of Mössbauer spec-troscopy (O'Hanley & Dyar 1993), $^{18}O/^{16}O$ and H/D analyses (Kyser et al., in prep.) on serpentine minerals, and studies on fluid inclusions found in several minerals in the associated rodingite (O'Hanley et al. 1992) are reported elsewhere. The original serpentine that formed at the expense of olivine was a lizardite mesh texture; it has undergone a complex series of recrystallization and replacement reactions, to be documented below.

Textures

Pseudomorphic textures after olivine

Lizardite-1T mesh and hourglass textures, as defined by Wicks & Whittaker (1977), are subdivided on the basis of observations reported at Cassiar. These different textures, particularly of the hourglass textures, form a record of the interaction of fluids with the serpentinite (O'Hanley et al. 1989b). Thus, they are not simply of academic interest, but provide the key information necessary to understand this complex process of serpentinization and recrystallization.

Lizardite-1T hourglass textures can be divided into type-1 and type-2 on the basis of extinction patterns within the mesh cells [see Wicks et al. (1977) for terminology]. In the type-1 texture, extinction sweeps continuously across the mesh cell and is asymptotic to sector boundaries. In the type-2 texture, extinction is discontinuous, owing to the presence of coarser crystallites in the mesh cell, and is not asymptotic to sector boundaries. The type-2 hourglass texture replaces the type-1 texture (Fig. 2a). Mesh textures also can be divided into types 1 and 2 based on the occurrence, in the mesh rims, of the same extinction characteristics as observed in the hourglass textures.

Serpentinites composed of type-1 hourglass texture also contain chrysotile + magnetite veins that have been pseudomorphically replaced by lizardite-1T contemporaneously with the lizardte-1T in the type-1 hourglass texture (Fig. 2b). In the normal sequence of alteration, olivine is replaced by lizardite, followed by the formation of chrysotile veins. The presence of lizardite pseudomorphs after chrysotile veins in the type-1 lizardite hourglass texture leads to two inferences: 1) the type-1 lizardite hourglass texture formed from a pre-existing serpentinite (Prichard 1979,

O'Hanley 1991), and 2) the reaction lizardite = chrysotile was reversed. Brucite was not observed in either thin section or microbeam studies of samples from any part of the serpentinite, with the exception of one sample of "bastite" (see Textures after enstatite, below).

Nonpseudomorphic textures after olivine

There are two types of serrate veins at Cassiar: 1) γ-serpentine serrate veins composed of chrysotile-$2M_{c1}$ and previously documented by Wicks & Whittaker (1977), and 2) α-serpentine serrate veins composed of lizardite-1T. Chrysotile serrate veins occur in interlocking textures (Wicks & Whittaker 1977) in the ore zone, where they are associated with antigorite and cut by veins of chrysotile asbestos. Serrate veins of lizardite are present in transitional textures (defined below) associated with ribbon veins or serrate veins of chrysotile located adjacent to, but outside, the ore zone. Serrate veins of lizardite recrystallize to form chrysotile and antigorite.

An unusual texture, characteristic of chrysotile asbestos deposits (Wicks & Whittaker 1977), seems to involve serpentine pseudomorphic after olivine in plane light but appearing as a featureless field of nearly isotropic lizardite-1T with no mesh cells in crossed nicols (Wicks & O'Hanley 1988: Figs. 20c and d). In some samples, this texture is associated with lizardite-1T serrate veins, lizardite-1T mesh texture and ribbon textures, which all pass into a lizardite + antigorite interlocking texture. This texture seems to be an incipient interlocking texture, transitional to a fully developed interlocking texture.

X-ray studies and observations in both incident and reflected light (see Wicks & Plant 1979) show that chrysotile + antigorite coexist without clinochlore in an interlocking texture after lizardite (Fig. 2c). Clinochlore occurs with antigorite having replaced both lizardite hourglass (Fig. 2d) and lizardite interlocking textures. Clinochlore without coexisting antigorite occurs in lizardite "bastite", and as a rim around relict ferrian chromite and chromite (Fig. 2e).

Lizardite + magnetite veins of variable width with cuspate vein-walls (Fig. 2e) cut the antigorite ± clinochlore interlocking texture and are in turn cut by veins of magnetite-free chrysotile asbestos. As the antigorite ± clinochlore texture has formed from lizardite-bearing textures, the existence of the lizardite–magnetite veins cutting the antigorite ± clinochlore texture indicates that a reaction involving the conversion of lizardite to antigorite ± clinochlore was reversed. Magnesite – lizardite – magnetite veins cut all other textures and veins and are located throughout the serpentinite. The magnesite – lizardite – magnetite veins are physically deformed, indicating that deformation continued after textural development of the serpentinite had ceased.
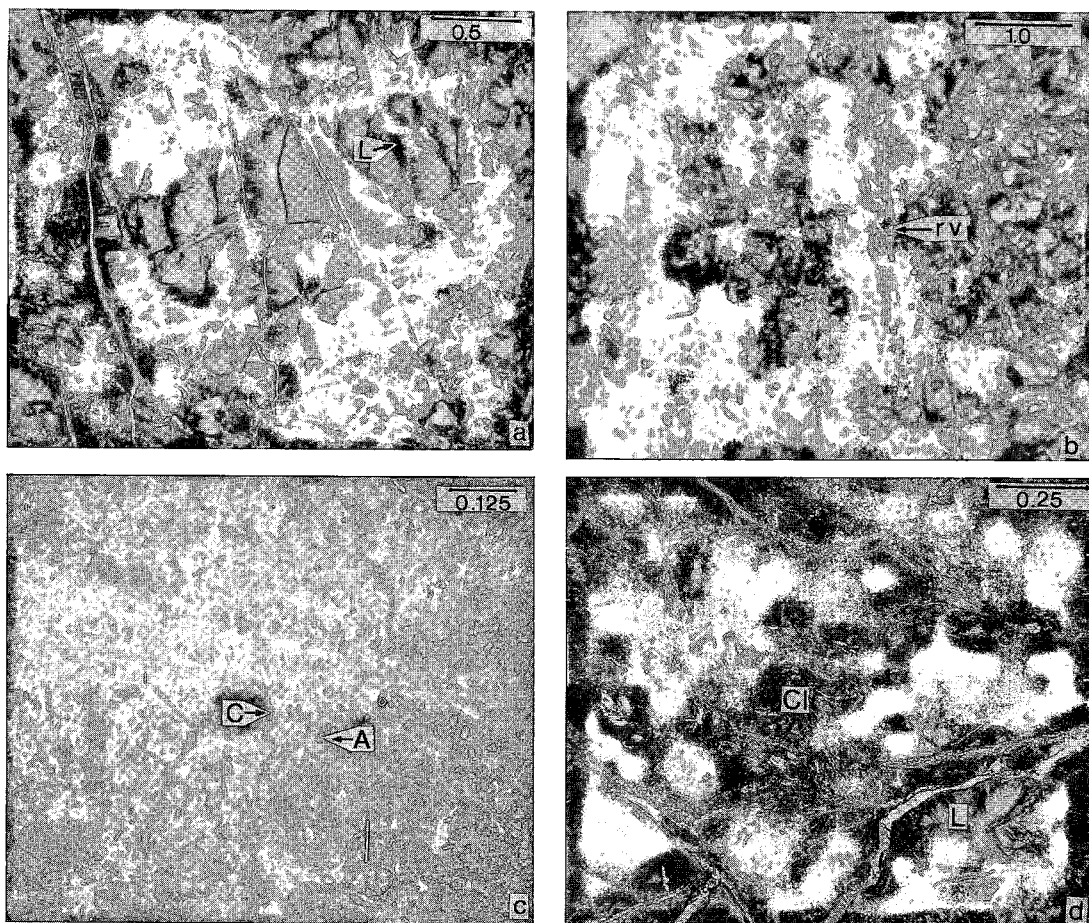
Textures after enstatite

At Cassiar, the serpentine pseudomorphs after enstatite ("bastite") have a continuous range of textures and mineralogy, and present an opportunity to solve some of the problems (such as the implications of the "bastite" texture) noted by Wicks & Whittaker (1977) and Wicks & Plant (1979). The textural types of "bastite" have been named, in order of increasing degree of recrystallization, uniform, domainal, patchy, shaggy, and indistinct. These are illustrated and discussed by Wicks & O'Hanley (1988). Uniform and domainal types of "bastite" consist of lizardite-1T. Some examples of domainal "bastite" in the hanging-wall serpentinite contain magnetite. Patchy "bastite" consists of lizardite-1T that was replaced by chrysotile-$2M_{c1}$. Shaggy and indistinct types of "bastite" consist of lizardite-1T, chrysotile-$2M_{c1}$, antigorite, and clinochlore. Brucite was identified by microbeam camera in one grain of patchy "bastite", associated with lizardite and antigorite.

Relationship between textures after olivine and those after enstatite

The relationship between the textures formed after olivine and those formed after enstatite is obscured, to the casual observer, by the diversity and complexity of serpentine textures. However, detailed observations from 93 thin sections clarify this relationship. A histogram (Fig. 3) relating each type of "bastite" to the serpentine texture after olivine that surrounds the "bastite" shows, in all but two examples, that there is only one serpentine texture after olivine surrounding a given grain of "bastite".

Uniform "bastite" comprises 42% of "bastite" grains associated with hourglass textures, but only 21% of the "bastite" grains associated with interlocking textures. Shaggy "bastite" comprises 35% of "bastite" grains associated with interlocking textures, but only 12% of the "bastite" grains with an hourglass texture. Domainal and patchy "bastite" occur in both textures, with domainal "bastite" slightly more common in hourglass textures, and patchy "bastite" slightly more common in interlocking textures.

Recrystallization of serpentinized olivine increases from mesh texture through to interpenetrating texture (Wicks & Whittaker 1977), e.g., hourglass textures are less strongly recrystallized than interlocking textures. Based on the correspondence between "bastite" textures and the texture of serpentine that replaced olivine adjacent to the "bastite", the extent of recrystallization of "bastite" increases from uniform to indistinct "bastite". However, during the recrystallization of patchy "bastite", chrysotile-$2M_{c1}$ formed, prior to antigorite, whereas in interlocking textures after olivine, lizardite recrystallized directly to form antigorite. In addition, the association of uniform

"bastite" with hourglass texture, and their presence in interlocking textures, suggest that "bastite" textures become modified at a different rate than serpentine textures after olivine. Thus, there is a general correspondence between serpentine textures after olivine and "bastite" textures, but in detail, serpentinized olivine and "bastite" evolved somewhat independently.

Spatial distribution of serpentine minerals and textures

The textural complexity of the Cassiar serpentinite is typical of chrysotile asbestos deposits (Wicks & Whittaker 1977). However, it is now possible to define the textural evolution of the Cassiar serpentinite on the basis of geological structure determined by detailed mapping. Mineral "isoregimes" for chrysotile and antigorite have been plotted on a geological map of the Cassiar serpentinite, along with a boundary between hourglass and transitional textures [the (type-1 Lz)–(type-2 Lz) boundary; Fig. 1] based on their first appearance. Lizardite persists in the most strongly

altered samples, indicating either that 1) lizardite is stable with chrysotile and antigorite, or 2) the reactions did not go to completion. We prefer the former alternative on the basis of complete destruction of the lizardite hourglass texture in the most strongly altered samples. If lizardite was not stable with chrysotile and antigorite, then lizardite would have been replaced when the hourglass texture was overprinted by chrysotile and antigorite. As lizardite persists in the interlocking texture with chrysotile and antigorite, we infer that it is stable (with a slightly modified composition: see below in Table 2).

In the southwestern corner of the mine, the serpentinite is composed only of type-1 lizardite hourglass texture after olivine, uniform and domainal "bastite", and accessory pyrrhotite and complex ferrian chromite – magnetite – serpentine grains (zone labeled T1Lz; Fig. 1). Type-1 lizardite hourglass texture has been recrystallized to type-2 lizardite hourglass texture, and lizardite serrate and ribbon veins. This marks the initiation of the change from hourglass (pseudomorphic) to interlocking (nonpseudomorphic) texture
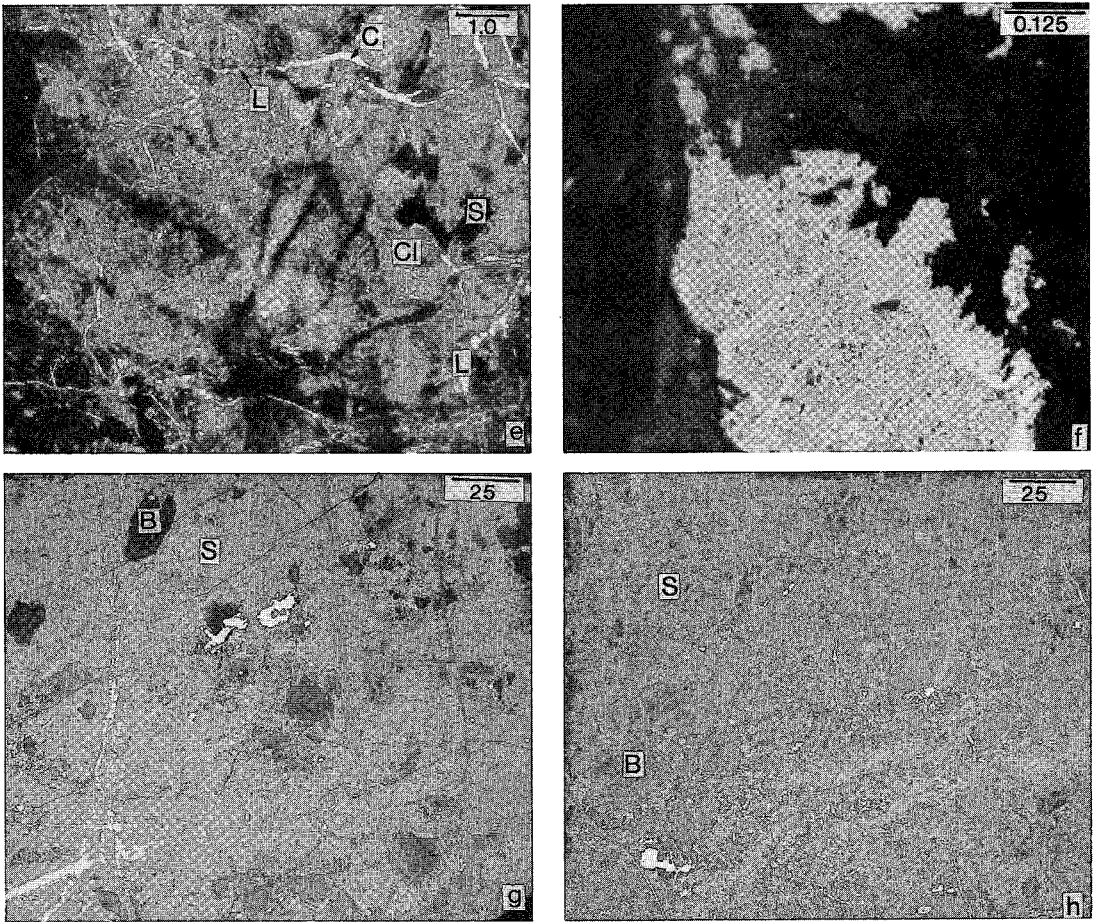
FIG. 2. Photomicrographs: all scale bars in millimeters. a) Type-1 lizardite hourglass texture being partly recrystallized to form type-2 lizardite hourglass texture, based on presence of crystallites (L) that disrupt extinction pattern (sample C56). b) Recrystallized chrysotile vein (rv), now lizardite-$1T$, with magnetite (C55). c) Antigorite (A) and chrysotile $2M_{c1}$ (C) in lizardite + chrysotile + antigorite interlocking texture, in reflected light (C20). d) Antigorite + clinochlore (Cl) after lizardite hourglass texture (L) (C71). e) Chrysotile asbestos veins (C) cut lizardite–magnetite veins (L) that cut antigorite–chlorite interlocking texture, with clinochlore (Cl) rimming relict chromite (S). (C112). f) Complex ferrian chromite – serpentine grain rimmed by magnetite, in reflected light (C20). g) and h) Alpha-track maps illustrating variations in boron content between "bastite" (B) and serpentine after olivine (S) based on a grey scale. Darker-colored minerals (e.g., "bastite") have higher concentrations of boron, whereas white-colored minerals (e.g., oxides) have little to none. In g), "bastite" contains more boron than does serpentine after olivine (C56), whereas in h), serpentine recrystallization has produced a uniform distribution of boron (C50).

(zone labeled type-2 Lz; Fig. 1).

Just west of the 45° shear and south of the 70° shear (Ctl and Atg zones; Fig. 1), lizardite ± antigorite ± clinochlore interlocking textures and lizardite ± chrysotile ± antigorite patchy "bastite", associated with uniform and domainal "bastite", replace the type-2 lizardite hourglass texture and the serrate veins and ribbon veins of lizardite. The association ferrian chromite – magnetite – serpentine is rarely present, and

magnetite grains are much more abundant. No sulfide minerals occur in thin sections of these samples. Although asbestos veins are present, they did not constitute ore owing to the springiness of the asbestos, which resulted in burst bags of milled fiber and unfavorable physical properties.

The ore zone lies north and east of these shear zones and consists of a lizardite ± chrysotile interlocking texture with chrysotile serrate veins ± antigorite ±
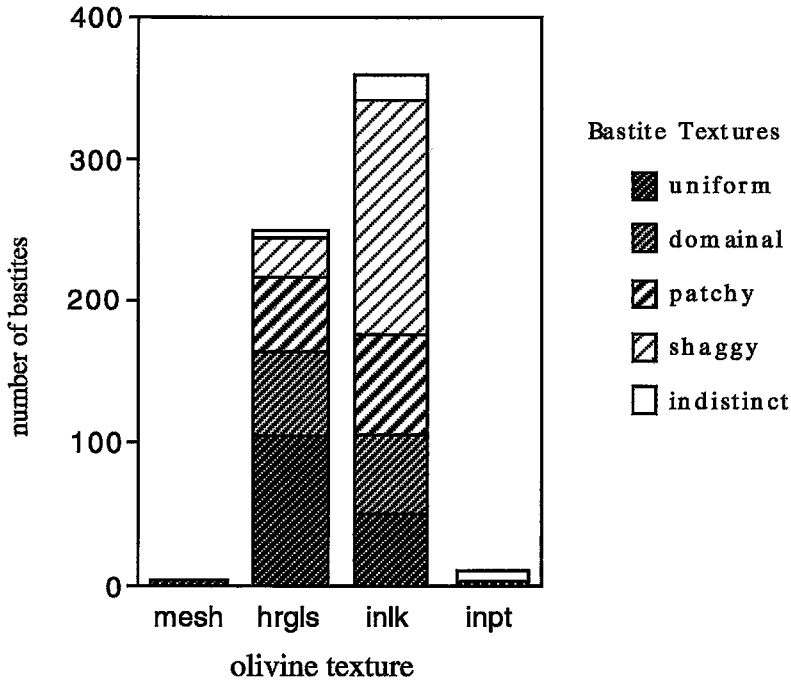
400 —

300 —

200 —

number of bastites

100 —

0 —

mesh hrgls inlk inpt

olivine texture

Bastite Textures

■ uniform

▨ domainal

▧ patchy

▨ shaggy

□ indistinct

FIG. 3. Correspondence between serpentine textures after olivine and those after enstatite. A plot of five "bastite" textures *versus* four serpentine textures after olivine (mesh: mesh texture, hrgls: hourglass, inlk: interlocking, inpt: interpenetrating). Two grains of "bastite" are surrounded by both pseudomorphic and nonpseudomorphic textures; both were plotted twice.

clinochlore ± magnetite ± heazlewoodite. Clinochlore mantles some relict grains of chromite. Relict lizardite pseudomorphic textures and relict ferrian chromite – magnetite – serpentine grains are present in the ore zone. "Bastite" varies from domainal to indistinct, with the indistinct "bastite" consisting of lizardite ± antigorite ± clinochlore.

There appears to be a continuous zone of antigorite along the 45° shear (Fig. 1), but a great deal of microbeam X-ray diffraction work will be required to delineate firmly the presence of this zone. Antigorite is difficult to recognize in interlocking textures in thin section; it is thus possible that the samples of interlocking texture that were not studied by X-ray diffraction also contain antigorite.

The distribution of clinochlore (for which an "isoregime" is not shown on Fig. 1) is different from that of antigorite. In particular, the orientation of the trend defined by samples containing clinochlore is oblique to the serpentine "isoregimes" near the 70° shear and perpendicular to that of the chrysotile "isoregime" at the southern end of the 45° shear (Fig. 1). In addition, antigorite was found in several samples without clinochlore, as indicated by the

divergence of the antigorite "isoregime" and clinochlore-bearing samples. In contrast to antigorite, clinochlore is easily identified in thin section by its interference color, so that the presence of antigorite without clinochlore is a sound interpretation.

The hanging-wall serpentinite, east of the ore zone, consists of mesh textures with lizardite and chrysotile mesh-rims and lizardite hourglass and isotropic mesh-centers. Uniform lizardite-$1T$, domainal lizardite-$1T$ (some with magnetite) and patchy lizardite-$1T$ – chrysotile-$2M_{c1}$ "bastite" also are present. Cobalt-rich pentlandite is the sulfide mineral (see below, Table 6, 6–7 to 6–11). Asbestos veins are absent.

An antigorite ± pentlandite interpenetrating texture occurs in the hanging-wall contact-alteration zone. It formed through the recrystallization of lizardite type-1 mesh texture (Wicks & O'Hanley 1988, Fig. 20d). Asbestos veins are absent.

Recrystallization through the various textures of lizardite to chrysotile and antigorite increases as the center of the serpentinite body is approached from either the east or the west. The change in mineral assemblages corresponds to the differences in hand samples. The yellow-green serpentinite that hosts the

ore zone has a transitional to interlocking texture consisting of lizardite, chrysotile and antigorite ± clinochlore ± heazlewoodite. The grains of "bastite" are shaggy to indistinct and consist of lizardite, chrysotile, antigorite ± clinochlore with relict oxides. In contrast, the black-veined, green serpentinite outside the ore zone consists of lizardite hourglass textures in the footwall serpentinite and lizardite mesh and hourglass textures in the hanging-wall serpentinite. Both contain magnetite veins ± pyrrhotite ± pentlandite + relict oxides. The "bastite" grains are uniform to patchy and consist of lizardite ± chrysotile ± magnetite.

The grey-green sugary serpentinite in the hanging-wall alteration zone is composed of antigorite ± lizardite interpenetrating texture ± pentlandite ± magnetite.

WHOLE-ROCK COMPOSITIONS

Whole-rock chemical analyses of samples of the ore zone, with and without clinochlore, and of the footwall serpentinite, indicate that, with the exception of small variations in both FeO and Fe_2O_3 contents, there is overall similarity in bulk composition (Table 1). In sample C112, the low SiO_2 and MgO totals and the high FeO and Fe_2O_3 totals can be attributed to a greater abundance of magnetite. The ore zone contains both less FeO and Fe_2O_3 (and hence less total Fe) than the footwall serpentinite.

MINERAL CHEMISTRY

Electron-microprobe data for the silicate minerals from the Cassiar serpentinite are shown in Tables 2 through 6. Rock-forming serpentine in samples C50 to C56, C139 and two samples of chrysotile asbestos (C167 and C200) were analyzed for Fe^{3+}/Fe^{2+} values by Mössbauer spectroscopy from powders obtained from hand samples (O'Hanley & Dyar 1993). Even though observations of thin sections were used to choose the location from which to take the samples, the Mössbauer values must be considered as representing whole-rock values because the analyzed powders may contain serpentine after both olivine and enstatite. In addition, antigorite is present in samples C50 to C52. As the presence of Fe^{3+} cannot be ignored, the microprobe analyses for both serpentine after olivine (Tables 2 and 3) and after enstatite (Table 4) were corrected on the basis of the Mössbauer data. In cases where no Mössbauer data are available, mineral formulae are shown with total iron as Fe^{2+}.

Lizardite and chrysotile

Both rock-forming (Table 2, analyses 2–1 to 2–10) and vein-forming (Table 2, 2–11 to 2–14) lizardites are similar in composition. In the footwall serpentinite in the southwest corner of the mine, lizardite has lost Fe^{3+} and gained Si during recrystallization from type-1

TABLE 1. REPRESENTATIVE WHOLE-ROCK COMPOSITIONS OF THE CASSIAR SERPENTINITE

| | Ore Zone serpentinite | | | | | | Footwall serpentinite | | |
| | with clinochlore | | | without clinochlore | | | | | |
	C20	C112	C121	C88	C90	C119	C54	C55	C56
SiO_2	39.30	34.90	39.10	39.40	38.90	38.60	39.50	38.8	38.60
TiO_2	0.04	0.04	0.04	0.05	0.04	0.04	0.04	0.04	0.04
Al_2O_3	1.15	0.98	1.14	0.74	0.98	0.86	1.15	1.00	1.06
Cr_2O_3	0.37	0.25	0.24	0.30	0.35	0.35	0.27	0.27	0.21
Fe_2O_3	3.42	11.97	2.94	2.74	4.34	4.57	3.25	5.75	5.03
P_2O_5	0.01	0.01	0.01	0.01	0.01	0.01	0.01	0.01	0.01
FeO	0.70	3.10	0.40	0.30	0.80	0.80	0.40	1.20	1.00
MnO	0.11	0.11	0.07	0.09	0.11	0.12	0.09	0.10	0.08
NiO	0.25	0.22	0.18	0.17	0.22	0.18	0.15	0.19	0.19
MgO	41.40	36.00	42.00	42.20	41.00	41.10	41.70	40.0	40.50
CaO	0.03	0.01	0.01	0.01	0.01	0.01	0.06	0.02	0.02
K_2O	0.01	0.01	0.02	0.02	0.02	0.01	0.02	0.01	0.01
Na_2O	0.20	0.18	0.19	0.23	0.18	0.18	0.20	0.16	0.29
L.O.I.*	13.40	11.60	13.50	13.90	13.50	13.30	13.40	12.50	13.00
Total	100.39	99.38	99.84	100.16	100.46	100.13	100.24	100.00	100.04

*L.O.I.: loss on ignition. Rb, Sr, Nb, and Ba present in amounts < 30 ppm. Compositions determined using X-ray fluorescence, and reported in wt.%.

TABLE 2. REPRESENTATIVE ELECTRON-MICROPROBE DATA ON LIZARDITE AND CHRYSOTILE

	1	2	3	4	5	6	7	8	9	10	11	12	13	14
SiO_2	39.79	41.64	40.36	40.82	39.09	39.45	40.34	39.68	39.78	40.19	37.95	39.51	39.41	40.07
TiO_2	0.05	0.00	0.00	0.04	0.04	0.04	0.02	0.06	0.04	0.04	0.03	0.05	0.03	0.05
Al_2O_3	0.89	0.80	1.36	1.34	0.90	0.75	0.68	0.79	1.07	0.87	1.52	1.64	1.06	1.18
Cr_2O_3	0.28	0.37	0.14	0.25	0.14	0.15	0.19	0.16	0.33	0.29	0.20	0.12	0.27	0.68
FeO	2.30	1.61	3.18	3.32	3.51	3.52	3.11	3.52	3.30	2.37	3.96	3.83	2.95	2.81
MnO	0.09	0.13	0.22	0.22	0.12	0.13	0.13	0.10	0.19	0.13	0.13	0.16	0.12	0.22
NiO	0.25	0.14	0.30	0.39	0.25	0.23	0.26	0.32	0.23	0.20	0.21	0.23	0.25	0.29
MgO	39.40	39.24	39.90	40.13	39.77	40.65	39.73	39.65	39.16	40.08	38.44	39.69	39.12	39.25
CaO	0.00	0.02	0.05	0.05	0.02	0.02	0.05	0.03	0.04	0.03	0.04	0.03	0.04	0.03
K_2O	0.02	0.02	0.05	0.06	0.04	0.03	0.04	0.03	0.03	0.03	0.03	0.03	0.03	0.04
Na_2O	0.01	0.00	0.06	0.06	0.02	0.03	0.06	0.04	0.07	0.07	0.04	0.03	0.06	0.04
Total	83.08	83.97	85.62	86.68	83.90	85.00	84.61	84.38	84.24	84.30	82.55	85.32	83.34	84.66

Formula based on 7 atoms of oxygens

	1	2	3	4	5	6	7	8	9	10	11	12	13	14
Si	1.96	1.99	1.94	1.94	1.92	1.94	1.96	1.94	1.94	1.95	1.90	1.93	1.95	1.94
$[IV]Fe^{3+}$	0.03	0.02	0.05	0.05	0.06	0.06								
$[IV]Al$	0.01	0.00	0.01	0.01	0.02	0.00								
Al							0.02	0.02	0.03	0.03	0.05	0.03	0.03	0.04
$[VI]Al$	0.02	0.02	0.03	0.03	0.01	0.02								
Cr	0.01	0.01	0.00	0.01	0.00	0.00	0.00	0.00	0.01	0.01	0.00	0.00	0.01	0.02
$[VI]Fe^{3+}$	0.02	0.02	0.05	0.06	0.06	0.06								
Fe^{2+}	0.04	0.02	0.02	0.02	0.03	0.03								
Fe							0.13	0.14	0.14	0.10	0.17	0.16	0.12	0.11
Mn	0.00	0.01	0.01	0.01	0.01	0.01	0.01	0.00	0.01	0.01	0.01	0.01	0.01	0.01
Ni	0.01	0.01	0.01	0.01	0.01	0.01	0.01	0.01	0.01	0.01	0.01	0.01	0.01	0.01
Mg	2.88	2.81	2.85	2.84	2.91	2.90	2.88	2.89	2.85	2.89	2.86	2.84	2.88	2.83

Cr/Al	0.333			0.429		0.429	
Fe^{2+}/Mg	0.009			0.005		0.005	
$Fe^{3+}_{Total}/(Si+Mg)$	0.009			0.015		0.016	

See Fig. 1 for sample locations. 1 and 2: Lizardite-1*T*, interlocking texture, sample C50; 3 and 4: Lizardite-1*T*, type-2 hourglass, C54; 5 and 6: Lizardite-1*T*, type-1 hourglass, C56; 7 and 8: Lizardite-1*T*, interlocking, C113; 9 and 10: Chrysotile-2M_{c1}, interlocking, C113; 11 and 12: Lizardite-1*T*, in lizardite-magnetite vein: 11: C20, 12: C56; 13 and 14: Lizardite-1*T*, type-1 hourglass, replaces chrysotile asbestos in vein, C56. Compositions reported in wt.% oxide.

(2–5, 2–6) to type-2 hourglass (2–3, 2–4) to interlocking texture (2–1, 2–2). However, the microprobe-derived compositions of chrysotile (2–9, 2–10) and lizardite (2–7, 2–8) in interlocking texture in the ore zone are similar, and both minerals have compositions similar to that of recrystallized lizardite in the footwall serpentinite. These analyses show that lizardite and chrysotile do not differ significantly in total Fe content, although O'Hanley & Dyar (1993) demonstrated that they do differ in Fe^{2+}/Fe^{3+} ratios. The Al content of both lizardite and chrysotile varies from 0.68 to 1.36 wt.% Al_2O_3. As the parent olivine must have had a very low Al content (Coleman & Keith 1971), the Al in these serpentines after olivine must have come from the breakdown of chromite (see oxides, Table 6) and the recrystallization of "bastite" (Table 4).

Lizardite in the footwall serpentinite (2–13, 2–14) that formed by replacement of chrysotile asbestos veins has the same composition as the rock-forming lizardite occurring next to it (2–5, 2–6). The vein lizardite from both the footwall serpentinite (2–12) and from the ore zone (2–11) contains slightly more Al and total Fe than the rock-forming lizardite and chrysotile after olivine.

Antigorite

Oxide values for antigorite were reduced to structural formulae using an assumed $M = 10$ (where $M = A/a$; A: superstructure wavelength; a: unit-cell parameter; Uehara & Shirozu 1985). This is a commonly occurring wavelength for antigorite and is convenient for comparing results of analyses.

Antigorite exhibits a greater variation in composition than lizardite or chrysotile because there are two different occurrences of antigorite at Cassiar (Table 3). Antigorite from the ore zone (analyses 3–1 to 3–6) has a composition similar to that of lizardite from the footwall serpentinite (2–1 to 2–6) except for slightly lower Fe contents (antigorite: 0.08 to 0.11 Fe per 7 atoms of oxygen; lizardite: 0.06 to 0.15 Fe per 7 atoms of oxygen). The lower Fe content of the antigorite is attributed to the formation of magnetite associated with antigorite crystallization.

Antigorite from the hanging-wall zone of alteration (3–7 to 3–9) has much higher Fe and lower Mg contents than antigorite in the ore zone. Sample C139 (3–7, 3–8) occurs closer to the contact between serpentinite and greenstone (Fig. 1) than does sample C141 (4–9). The greater amounts of modal antigorite, antigorite needles replacing pentlandite and the absence of magnetite in C139 suggest a greater degree of recrystallization than in C141. The higher Fe content in C139 (compared to that in C141) is consistent with its more intense recrystallization.

"Bastite"

Grains of "bastite" (Table 4) have a slightly higher Cr content than serpentine formed at the expense of olivine (Tables 2, 3), probably reflecting the Cr content of the original enstatite. Lizardite in uniform (4–9, 4–10) and domainal (4–3, 4–6) textures has a higher Fe and lower Mg, Cr, and Al content than lizardite (4–1, 4–2, 4–4, 4–7, 4–8) and chrysotile (4–5) in patchy textures. Clinochlore occurs in shaggy (4–12, 4–13) and indistinct "bastite", although there is also a chlorite-like mineral in patchy "bastite" (thin-section observation) that only contains 7 wt.% Al_2O_3 (4–9). Clinochlore contains the highest concentrations of Cr of the silicate phases (4–12, 4–13).

Comparison between lizardite after olivine and lizardite after enstatite

The textural and mineralogical evidence suggests that the serpentines after olivine and after enstatite evolved somewhat independently of each other. Mineral compositions can be used to test this conclusion by establishing the presence or absence of equilibrium between serpentine derived from different hosts. For example, equilibrium can be examined by calculating cation ratios, such as Fe^{2+}/Mg, for coexisting lizardite after olivine and that after enstatite. If chemical equilibrium exists, then on a plot of Fe^{2+}/Mg in lizardite after olivine *versus* Fe^{2+}/Mg in lizardite after enstatite, the data points should plot on the diagonal.

The values of Fe^{2+}/Mg (Fig. 4a), Cr/Al (Fig. 4b) and $Fe^{3+}/(Mg + Si)$ (Fig. 4c) for samples C50 to C56, all from the footwall serpentinite, represent the transition from the least-recrystallized sample (C56) through samples exhibiting intermediate amounts of recrystallization (with increasing amounts of recrystallization from sample C55 to C51) to the most-recrystallized sample (C50). Arrows between successive samples in Figure 4 point in the direction of increasing amounts of recrystallization.

In the case of Fe^{2+}/Mg (Fig. 4a), the points representing slightly less (C52) and slightly more (C50) recrystallization do not plot on the diagonal, so that the location of C51, which does, is probably fortuitous. The Cr/Al values exhibit a trend toward the diagonal with increasing recrystallization, but the points do not plot on the diagonal (Fig. 4b). The data for $Fe^{3+}/(Mg + Si)$ also exhibit a trend toward the diagonal with increasing recrystallization (Fig. 4c). The three points representing the most intense recrystallization (C52 to C50) plot near or on the diagonal. The data indicate that although equilibrium has not been established at Cassiar, it was approached with increasing recrystallization.

The values of Fe^{2+}/Mg (Fig. 4a), Cr/Al (Fig. 4b) and $Fe^{3+}/(Mg + Si)$ (Fig. 4c) all indicate an increase in uniformity of composition with an increase in the extent of recrystallization and replacement. Another

TABLE 3. REPRESENTATIVE ELECTRON–MICROPROBE DATA ON ANTIGORITE

	1	2	3	4	5	6	7	8	9
SiO_2	40.70	40.71	40.38	40.48	37.23	40.30	42.78	42.57	41.55
TiO_2	0.00	0.01	0.05	0.02	0.02	0.04	0.06	0.06	0.02
Al_2O_3	1.50	1.12	1.94	1.54	6.81	1.27	0.66	0.84	0.17
Cr_2O_3	0.04	0.20	0.15	0.11	0.70	0.59	0.47	0.69	0.36
FeO	2.99	2.08	2.34	2.39	2.10	2.67	6.31	5.92	3.43
MnO	0.19	0.13	0.16	0.19	0.16	0.19	0.33	0.26	0.25
NiO	0.17	0.16	0.29	0.27	0.27	0.26	0.21	0.24	0.17
MgO	39.49	40.25	39.82	39.20	37.78	40.80	36.49	36.84	38.63
CaO	0.04	0.02	0.03	0.04	0.06	0.05	0.05	0.05	0.04
K_2O	0.01	0.02	0.03	0.04	0.03	0.03	0.04	0.03	0.04
Na_2O	0.03	0.04	0.05	0.05	0.07	0.09	0.03	0.05	0.02
Total	85.17	84.74	85.24	84.33	85.23	86.29	87.43	87.55	84.68

Formula based on 6.8 atoms of oxygen[a]

Si	1.87	1.92	1.88	1.94	1.74	1.86	1.99	1.96	1.94
$^{[V]}Fe^{3+}$	0.04	0.03	0.04	0.04			0.02	0.02	
$^{[IV]}Al$	0.06	0.03	0.05	0.02					
Al					0.19	0.04			0.02
$^{[VI]}Al$	0.00	0.00	0.00	0.02			0.02	0.02	
Cr	0.00	0.00	0.00	0.00	0.01	0.01	0.01	0.01	0.01
$^{[VI]}Fe^{3+}$	0.03	0.02	0.03	0.03			0.04	0.03	
Fe^{2+}	0.04	0.03	0.02	0.02			0.19	0.18	
Fe					0.08	0.10			0.13
Mn	0.08	0.01	0.01	0.01	0.01	0.01	0.01	0.01	0.01
Ni	0.01	0.01	0.01	0.01	0.01	0.01	0.01	0.01	0.01
Mg	2.70	2.84	2.77	2.67	2.62	2.81	2.51	2.53	2.68
Fe^{2+}/Mg	0.01	0.01	0.01	0.01			0.08	0.07	

[a] See text for justification of 6.8 atoms of oxygen per formula. See Figure 1 for sample locations. Ore zone: 1 and 2: antigorite, interlocking texture, sample C50; 3 and 4: antigorite, interlocking, C51; 5 and 6: antigorite, interlocking, C113. Hanging-wall alteration zone: 7 and 8: antigorite, interpenetrating, C139; 9: antigorite, interpenetrating, C141.

TABLE 4. REPRESENTATIVE ELECTRON-MICROPROBE DATA ON "BASTITE"

	1	2	3	4	5	6	7	8	9	10	11	12	13
SiO_2	38.89	39.64	39.67	39.36	39.87	39.59	39.91	40.00	40.00	40.37	36.10	32.04	31.66
TiO_2	0.00	0.03	0.05	0.02	0.02	0.05	0.04	0.02	0.01	0.03	0.05	0.07	0.07
Al_2O_3	0.86	1.29	1.50	0.84	1.06	1.37	1.22	1.38	1.29	1.07	7.69	13.97	13.54
Cr_2O_3	0.57	0.52	0.52	0.60	0.60	0.91	0.60	0.78	1.04	0.84	1.97	2.61	2.70
FeO	1.53	2.10	2.57	1.61	1.68	2.95	2.00	2.31	2.46	2.31	2.58	2.96	3.05
MnO	0.25	0.22	0.24	0.20	0.14	0.24	0.20	0.30	0.17	0.15	0.18	0.18	0.13
NiO	0.21	0.26	0.31	0.17	0.26	0.24	0.27	0.25	0.25	0.26	0.28	0.24	0.31
MgO	39.72	39.12	39.31	39.76	40.13	38.84	39.78	39.80	39.27	39.23	36.99	33.87	34.11
CaO	0.02	0.02	0.07	0.04	0.00	0.03	0.05	0.05	0.01	0.04	0.04	0.03	0.03
K_2O	0.02	0.02	0.03	0.02	0.02	0.03	0.04	0.05	0.04	0.04	0.04	0.04	0.04
Na_2O	0.04	0.04	0.07	0.13	0.09	0.04	0.05	0.07	0.06	0.10	0.02	0.04	0.07
Total	82.11	83.26	84.34	82.75	83.87	84.29	84.16	85.01	84.60	84.44	85.94	86.05	85.71

Formula based on 7 atoms of oxygens

	1	2	3	4	5	6	7	8	9	10	11	12	13
Si	1.93	1.95	1.93	1.94	1.94	1.94	1.94	1.93	1.94	1.96	1.73	1.54	1.54
$^{[IV]}Fe^{3+}$	0.02	0.03	0.04	0.03	0.02	0.04	0.03	0.04	0.04	0.04			
$^{[IV]}Al$	0.02	0.02	0.03	0.02	0.03	0.02	0.03	0.03	0.02	0.00			
Al											0.22	0.40	0.39
$^{[VI]}Al$	0.00	0.02	0.01	0.00	0.00	0.02	0.01	0.01	0.02	0.03			
Cr	0.01	0.01	0.01	0.01	0.01	0.02	0.01	0.01	0.02	0.02	0.04	0.05	0.05
$^{[VI]}Fe^{3+}$	0.02	0.02	0.04	0.03	0.03	0.04	0.04	0.04	0.04	0.04			
Fe^{2+}	0.02	0.04	0.02	0.02	0.02	0.01	0.01	0.01	0.02	0.02			
Fe											0.10	0.12	0.13
Mn	0.01	0.01	0.01	0.01	0.01	0.01	0.01	0.01	0.01	0.01	0.01	0.01	0.01
Ni	0.01	0.01	0.01	0.01	0.01	0.01	0.01	0.01	0.01	0.01	0.01	0.01	0.01
Mg	2.95	2.86	2.86	2.93	2.91	2.84	2.88	2.86	2.83	2.83	2.64	2.43	2.46
Cr/Al		0.333		0.222		0.182			0.143			0.200	
Fe^{2+}/Mg		0.009		0.009		0.009			0.007			0.009	
$Fe^{3+}_{Total}/(Mg+Si)$		0.009		0.018		0.017			0.022			0.026	

1 and 2: Lizardite-1T, patchy texture, sample C50; 3: Lizardite-1T, domainal, C51; 4: Lizardite-1T, patchy, C52; 5: Chrysotile-2M_{c1}, patchy, C52; 6: Lizardite-1T, domainal, C54; 7 and 8: Lizardite-1T, patchy, C54; 9 and 10: Lizardite-1T, uniform, C56; 11: chlorite-like mineral, shaggy, C112. 12 and 13: Clinochlore, shaggy, C112. See Fig.1 for sample locations.

indication of greater compositional uniformity between serpentine after olivine and that after enstatite with increasing recrystallization and replacement is provided by the distribution of boron (B). The results for samples C50 to C56 indicate a continuous change in B distribution with increasing recrystallization. The contrast in B content between lizardite after olivine and that after enstatite in C56, the least-recrystallized (Fig. 2g), and the absence of contrast between these textural elements in C50, the most intensely recrystallized (Fig. 2h) serpentinite, document the increasing uniformity in the distribution of B with increasing recrystallization.

The change in cation ratios and in the distribution of B between serpentine after olivine and that after enstatite suggests that the two changed independently early in recrystallization but approached similar values as extent of recrystallization increased. The similarity in composition between "bastite" and matrix serpentine can be attributed to a large extent of recrystallization on the basis of earlier discussion of serpentine textures.

Sulfides

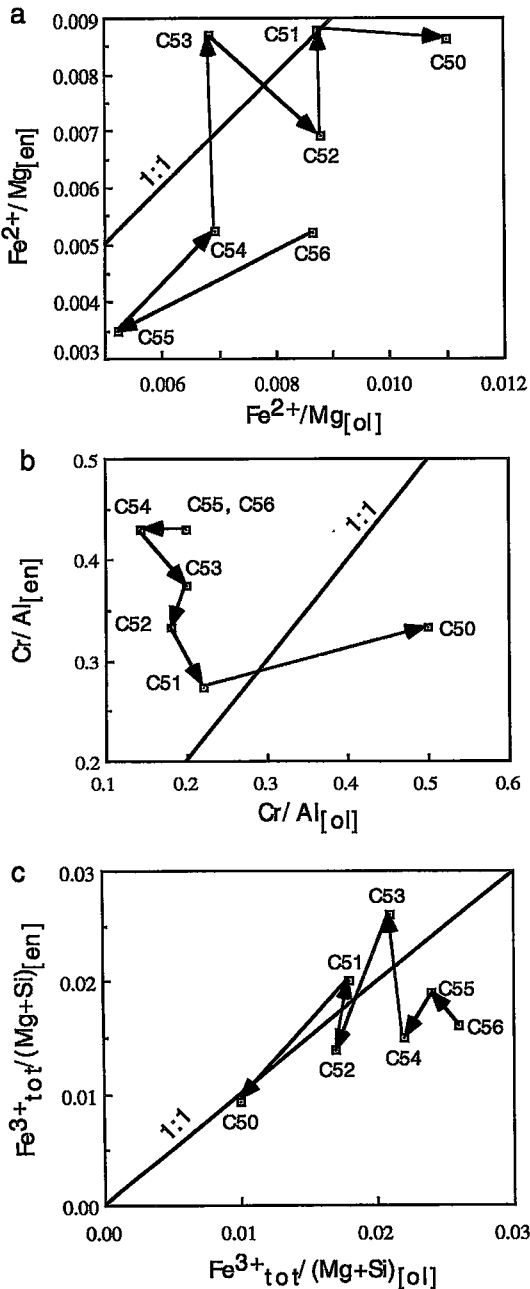Sulfides are rare in the Cassiar serpentinite, occurring as discrete monomineralic grains. Pentlandite

FIG. 4. Comparison of Fe^{2+}/Mg (a), Cr/Al (b), and $Fe^{3+}/(Mg + Si)$ (c) values in lizardite after olivine and lizardite after enstatite, using data for samples C50 to C56 taken from Tables 2 and 4.

(Table 5, 5–6 to 5–11) occurs in the hanging-wall serpentinite and is the most abundant sulfide (but still much less than 1 vol.%). Antigorite has replaced

pentlandite in the hanging-wall zone of alteration; the latter mineral thus predates the formation of antigorite. Therefore, the variation in Co content of pentlandite, from C151 (5–9 to 5–11) to C139 (5–5 to 5–8), over a distance of 30 meters, also must predate antigorite. Pyrrhotite is associated with hourglass textures in the footwall serpentinite, whereas heazlewoodite (5–1 to 5–5) is associated with nonpseudomorphic textures in the ore zone.

Oxides

Magnetite is the most abundant oxide mineral in the Cassiar serpentinite; it is present in virtually all rock and vein textures. Most of the magnetite in the rocks contains Cr, varying from 0.48 to 4.54 wt.% Cr_2O_3 (Table 6), and its composition does not change progressively with degree of recrystallization. In contrast, magnetite in the veins contains less than 1 wt.% Cr_2O_3 (O'Hanley *et al.* 1992). Oxide minerals exhibit a complex pattern in most samples, as illustrated by a chromite–serpentine intergrowth surrounded by magnetite (Fig. 2f). The chromite cores are mantled by magnetite or by chromian magnetite. Results of electron-microprobe analyses of the cores were found to be unsatisfactory because serpentine inclusions produced low totals. However, the compositions of the cores are clear from the analyses, and they are presented here because they indicate that the composition of the cores ranges from chromite (6–1) to ferrian chromite (6–3, 6–7) and because they illustrate the migration of elements during serpentinization. The chromite cores lost both Al and Cr during recrystallization.

PROPOSED REACTIONS RELATING
MINERAL ASSEMBLAGES

The serpentinites at Cassiar are very fine-grained rocks. Previous studies of serpentinites other than at Cassiar (Wicks & Whittaker 1977) have shown that in some serpentinites, such as hourglass-texture serpentinites, one can be reasonably confident that the rock is composed of lizardite. In other serpentinites, such as those composed of interlocking textures, the mineralogy is complex, and detailed microbeam X-ray-diffraction studies are necessary to identify the various serpentine minerals. At Cassiar, where interlocking textures are so abundant, it was not feasible to do the enormous amount of microbeam X-ray work required to make estimates of the mineral modes in thin sections. Therefore, the discussions of chemical reactions that follow are necessarily qualitative because they are based on inferred, not measured, modes.

Changes in mineral assemblages at Cassiar can be described qualitatively by the reactions shown in Table 7. The reactions (1 to 5) involving conversion of

TABLE 5. REPRESENTATIVE ELECTRON-MICROPROBE DATA ON SULFIDES*

	1	2	3	4	5	6	7	8	9	10	11
Cr	0.07	0.09	0.10	0.03	0.30	0.04	0.04	0.09	0.06	0.05	0.03
Fe	0.11	0.10	0.07	0.09	0.11	24.51	24.11	23.43	20.46	20.69	20.46
Ni	59.97	59.96	60.10	58.75	52.11	27.31	27.94	28.63	31.32	30.74	30.98
Cu	0.16	0.15	0.24	0.09	0.10	0.03	0.08	0.03	0.07	0.03	0.11
Co	0.12	0.08	0.04	0.04	0.07	1.44	1.48	1.43	1.75	1.73	1.75
S	39.57	39.62	39.44	41.00	41.58	46.66	46.30	46.36	46.35	46.76	46.66

See Fig. 1 for sample locations. *Totals have been normalized to 100%. 1, 2, and 3: Heazlewoodite, sample C20. 4 and 5: Heazlewoodite, C113. 6, 7, and 8: Pentlandite, C139. 9, 10, and 11: Pentlandite, C141.

olivine and enstatite to form type-1 lizardite are postulated on the basis of observations at Cassiar and from many other serpentinites (*e.g.*, Hostetler *et al.* 1966, Dungan 1979, O'Hanley & Offler 1992). The production of brucite early in the serpentinization of harzburgite is attributed to the reaction olivine + H_2O = lizardite + brucite (reaction 1), rather than olivine + enstatite + H_2O = lizardite. The delayed serpentinization of enstatite produces only lizardite (reaction 2), and releases SiO_2, which combines with brucite to form more lizardite (reaction 3). The oxidation of Fe^{2+} to form magnetite with chrysotile (reaction 4) and the replacement of chrysotile by lizardite in the early-formed veins (reaction 5) are additional reactions that operate to form the footwall serpentinite.

The sequence of changes from type-1 to type-2 lizardite hourglass to lizardite + antigorite interlocking texture can be described by reactions 6 and 7 (Table 7), in which lizardite formed from both serpentinized olivine and enstatite, together with relict chromite, recrystallized to new lizardite + antigorite ± magnetite over a distance of approximately 80 meters west of the 45° shear (Fig. 1).

The transition in the ore zone from lizardite ± pentlandite to chrysotile ± antigorite ± clinochlore ± heazlewoodite is complex because the development of clinochlore seems to be superimposed onto the process of serpentinization. Clinochlore bears no relationship to the sequence of serpentinization deduced from the textural patterns west of the 45° shear. In the ore zone, clinochlore replaced the lizardite hourglass texture as well as the lizardite interlocking texture, so that it seems to have formed from minerals in both textures, rather than forming from a transitional texture only. The high Cr and Al content of clinochlore [compare the composition of lizardite (2–7, 2–8) and antigorite (3–5, 3–6) to clinochlore (4–12, 4–13)] indicates that the breakdown of chromite was important in the formation of clinochlore because the required Al could not have come only from lizardite.

Reactions 8 to 11 are proposed to describe the formation of textures in the ore zone; these reactions are basically the same as those that describe the breakdown of the type-1 hourglass textures (reactions 6 and 7). The absence of talc in the pre-antigorite + clinochlore assemblage, of brucite in the antigorite + clinochlore assemblage, and the presence of talc + magnetite within the 45° shear, suggest that SiO_2 was added to the system, *i.e.*, on the reactant side of reactions 8 and 10 (Table 7). The reaction of pentlandite and pyrrhotite to produce heazlewoodite (11) can be described as $(Fe,Ni)S + O_2 = NiS$ + magnetite.

TABLE 6. REPRESENTATIVE ELECTRON-MICROPROBE DATA ON OXIDES

	1	2	3	4	5	6	7	8	9	10	11
TiO_2	0.17	0.10	0.10	0.20	0.12	0.15	0.18	0.16	0.16	0.17	0.19
Al_2O_3	14.47	0.08	0.28	0.01	0.17	0.20	3.22	0.12	0.14	0.20	0.16
Cr_2O_3	41.79	2.00	22.09	4.00	4.54	2.80	31.35	1.25	0.48	9.29	3.07
FeO	29.84	95.48	65.40	89.35	85.43	90.92	53.71	92.91	93.06	85.56	91.14
MgO	5.96	1.27	1.39	0.38	1.73	0.78	2.42	0.94	0.18	0.27	0.14
Total*	92.23	98.93	89.26	93.94	91.99	94.85	90.88	95.38	94.02	95.49	94.70

*Low totals due to silicate inclusions. See Fig. 1 for sample locations. 1: chromite, C20. 2: chromian magnetite, C20. 3: ferrian chromite, C50. 4: chromian magnetite, C50. 5 and 6: chromian magnetite, C56. 7: ferrian chromite, C113. 8: chromian magnetite, C113. 9: magnetite, C141. 10 and 11: chromian magnetite, C141.

TABLE 7. POSTULATED SERPENTINE REACTIONS IN THE CASSIAR SERPENTINITE

Inferred from thin section	System $MgO-SiO_2-H_2O$

Initial serpentinization

Ol + En to Type-1 Lz hourglass texture & Lz "bastite"

1. (mesh): $Ol^{**} + H_2O + O_2 = Lz + Brc + Mgt$	$Fo + H_2O = Lz + Brc$
2. ("bastite") $En + H_2O = Lz + SiO_{2(aq)}$	$En + H_2O = Lz + SiO_2$
3. (type-1 hourglass) $Brc + SiO_2 + H_2O = Lz$	$Brc + SiO_2 + H_2O = Lz$
4. (vein) $Lz + O_2 = Ctl + Mgt$	$Lz = Ctl$
5. (vein) $Ctl = Lz$	$Ctl = Lz$

Composite Reaction
$$Ol + En + 3 H_2O + O_2 = 3 Lz + 2 Mgt \qquad\qquad Fo + En + H_2O = Lz$$

Footwall adjacent to $45°$ shear

Type-1 Lz hourglass to Type-2 Lz hourglass to Lz + Atg interlocking texture

6. type-1 $Lz + Chm + O_2 = $ type-2 $Lz + Mgt$	change in texture
7. type-2 $Lz + SiO_2 + O_2 = Atg + Mgt$	$Lz + SiO_2 = Atg$

Composite Reaction
$$\text{type-1 } Lz + Chm + SiO_2 + O_2 = Atg + 2 Mgt \qquad\qquad Lz + SiO_2 = Atg$$

Ore Zone

Type-2 Lz hourglass texture to Ctl + Atg interlocking texture

8. $Lz + Chm + SiO_2 + O_2 = Atg + Cl + Mgt$	$Lz + SiO_2 = Atg$
9. $Lz = Ctl$	$Lz = Ctl$
10. $Lz + SiO_2 = Atg$	$Lz + SiO_2 = Atg$
11. $(FeNi)S + O_2 = Ni_3S_2 + Mgt + S_2$	not applicable

Composite Reaction
$$3 Lz + Chm + (FeNi)S + 2 SiO_2 + 2 O_2 = \qquad\qquad 3 Lz + 2 SiO_2 =$$
$$2 Atg + Ctl + 2 Mgt + Ni_3S_2 + S_2 \qquad\qquad 2 Atg + Ctl$$

Hangingwall Contact-Alteration Zone

Lz mesh-rim texture to Atg interpenetrating texture

12. $Lz + SiO_2 + (FeNiCo)S + Mgt =$	$Lz + SiO_2 = Atg$
$Atg + S_2 + O_2$	

* Reactions are based on observed changes in mineralogy from thin section. Reactions are schematic because mineral modes could not be estimated from thin section. Composite reactions are based on the sum of the individual reactions listed for each transition. ** Abbreviations: Ol: olivine; Fo: forsterite; Lz: lizardite; Brc: brucite; Mgt: magnetite; En: enstatite; Ctl: chrysotile; Chm: chromite; Cl: clinochlore.

Sulfides are not sufficiently abundant in the samples to be more specific. The replacement of pentlandite by heazlewoodite is typical of highly serpentinized rocks (*e.g.*, Shiga 1987).

The development of the hanging-wall contact-alteration zone is distinct from the development of the ore zone. Antigorite overprints a partially recrystallized lizardite mesh-rim texture. Lizardite, pentlandite, and magnetite were destabilized during the formation of antigorite, yielding a nearly monomineralic zone of antigorite (reaction 12; Table 7).

DISCUSSION

Phase diagram for the serpentines

The changes in serpentine mineralogy at Cassiar can be modeled to a first approximation using the system $MgO–SiO_2–H_2O$ (MSH). This simple system can be used for the following reasons. First, Mn, Ni, Cr and Al values are either very low or similar in all three serpentine minerals, and thus were not important in their stabilization. Second, clinochlore, which is

enriched in Cr and Al with respect to the serpentine minerals, was produced by the breakdown of relict chromite and not from the breakdown of any of the serpentine minerals. Thus, it need not be included in the system. Third, electron-microprobe and Mössbauer data from the serpentine minerals at Cassiar show that even though Fe is the most abundant element substituting in the serpentine structure, the extent of its incorporation is minimal. The variations range from 0.02 to 0.06 Fe^{3+} for Si, 0.02 to 0.06 Fe^{3+} for Mg and 0.02 to 0.04 (excluding the antigorite from the zone of hanging-wall alteration) Fe^{2+} for Mg. Magnetite can be either a reactant or a product when lizardite reacts to form antigorite, and modal magnetite can change when lizardite recrystallizes to form a new lizardite texture (O'Hanley & Dyar 1993). Changes in modal magnetite are reflected in changes in the total Fe content as well as in the ratios Fe^{3+}/Fe_{total} and $^{[VI]}Fe/(^{[VI]}Fe + Mg)$ in lizardite, suggesting that these changes are related to changes in the activity of silica, $a(SiO_2)$, rather than changes in P and T (O'Hanley & Dyar 1993).

These observations show that it is not essential to include magnetite in a model proposed to estimate P and T for the serpentine reactions in the Cassiar serpentinite. However, it is an assumption to consider lizardite and chrysotile to be polymorphs in the MSH system. This assumption is not supported by the observations at Cassiar, where lizardite has persisted during the formation of chrysotile and antigorite, and all three minerals have distinct compositions when Mössbauer data are used to assign Fe^{2+} and Fe^{3+} to coordination sites (see O'Hanley & Dyar 1993). However, the importance of Fe^{3+} incoporation in chrysotile has not yet been evaluated (studies are in progress). The change in composition from lizardite to chrysotile necessitates the presence of either another mineral phase or ions to complete the mass balance. However, for the purposes of estimating the T and P of formation, we believe that the small extents of Fe incorporation in the serpentine minerals at Cassiar have a negligible effect on molar entropies and volumes, and can be ignored to a first approximation.

The approximation that lizardite and chrysotile have similar compositions has two implications: first, lizardite forms metastably after olivine, and second, the system $MgO-Al_2O_3-SiO_2-H_2O$ (MASH) used by O'Hanley et al. (1989a) is unnecessary for compositions at Cassiar. If lizardite and chrysotile are polymorphs, then only one of them can form stably after olivine. Chrysotile is considered stable in this system for the reasons given by O'Hanley (1991). Two of the key equilibria in the MASH model, namely, the reactions lizardite = chrysotile + chlorite and lizardite + talc = antigorite + chlorite, did not operate at Cassiar, indicating that the MASH model is not applicable to the phase relations in the Cassiar serpentinite.

A model of the phase diagram for serpentine in the MSH system has been presented by O'Hanley et al.

(1989a) based on optimized thermodynamic data of Berman (1988), as modified by Chernosky et al. (1988), and topologic constraints of O'Hanley (1987). This diagram, modified by the addition of enstatite to the chemography, is shown in Figure 5. Although topologically correct, the locations of the lizardite-bearing equilibria are only schematic because they are constrained topologically to temperatures below the corresponding chrysotile-bearing equilibrium. The lack of data for the end-member magnesian lizardite precludes calculation of lizardite-bearing equilibria.

O'Hanley et al. (1989b) calculated temperatures of serpentinization using the serpentine–magnetite oxygen-isotope thermometer of Wenner & Taylor (1971) on chrysotile asbestos – magnetite veins, and lizardite – magnetite from a magnesite – lizardite – magnetite vein. These samples span the entire range of textures and, therefore, bracket the temperatures of recrystallization and replacement. The calculated temperatures vary from 265 to 350°C for asbestos–magnetite veins to 307°C for a lizardite–magnetite vein, and suggest that recrystallization was isothermal at 300 ± 50 °C. Using a corrected version of the thermometer based on the published quartz–water fractionation factor of Clayton et al. (1972), the measured fractionations yield temperatures of 250 ± 25 °C.

Fluid inclusions found in clinozoisite, grossular, and diopside, the principal minerals of rodingites, which span the recrystallization event, have homogenization temperatures of 276 ± 36°C, and salinities of 8 ± 1.2 equiv. wt.% NaCl (O'Hanley et al. 1992). The freezing temperatures, –30°C to –50°C, and the failure of a clathrate to form when the inclusions are cooled below –100°C, indicate that the fluid is primarily of aqueous composition, with <0.85 mol % CO_2. A $P(H_2O)$ of less than 800 bars during the recrystallization event was determined using the temperature inferred from the isotopic data to correct the homogenization temperatures along the appropriate isochore (O'Hanley et al. 1992). Using the revised estimates of temperature increases the upper estimate for $P(H_2O)$ to 1 kbar. Thus, serpentine recrystallization and replacement occurred at 250 ± 25 °C and <1 kbar. These ranges of temperature and pressure are shown as a box on Figure 5. The fluid-inclusion data, the absence of carbonate minerals in the serpentinite, the scarcity of sulfide minerals, the localization of talc in the 45° shear, and the fact that all serpentine recrystallization and replacement took place in a completely hydrated peridotite support the hypothesis that $a(H_2O)$ was approximately equal to 1.

The serpentine reactions at Cassiar have been modified to conform with the MSH system and are listed in Table 7. The changes in serpentine mineralogy at Cassiar can be explained by two stages of serpentinization in the following manner. The first stage, hydration of the peridotite, is no longer recorded at Cassiar because there is no relict olivine, and the least-
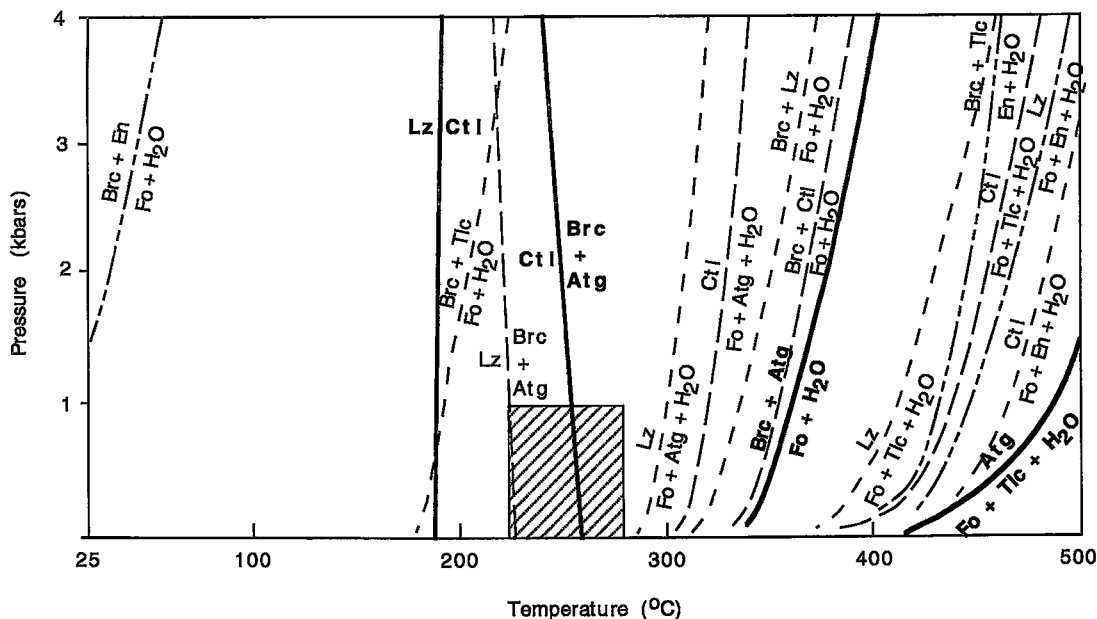
FIG. 5. A portion of the P(H₂O)–T diagram for the serpentine minerals lizardite (Lz), chrysotile (Ctl), and antigorite (Atg), and other relevant phases, in the system MgO–SiO₂–H₂O. The other phases are: brucite (Brc), forsterite (Fo), enstatite (En), talc (Tlc), and H₂O. Stable reactions are represented by bold solid lines, metastable reactions by long-dashed lines, doubly metastable reactions by short-dash lines, and triply metastable reactions by long- and short-dashed lines. (Levels of metastability refer to assemblages representing different values for the free energy at a given point in composition space: the assemblage with the lowest free energy is stable; the assemblages with the next-lowest free energy is metastable; the assemblage with the third-lowest free energy is doubly metastable, *etc*.) Lizardite-bearing equilibria are shown in topologically correct positions only. All other equilibria were calculated using GEØCALC (Berman *et al.* 1986) and the thermodynamic dataset of Berman (1988). The box represents the estimated range of conditions of temperature and pressure for serpentine recrystallization and replacement at Cassiar.

recrystallized textures (hourglass textures) formed from a previously existing serpentinite. Therefore, we cannot specify the relevant reactions on the basis of data from the mine. However, the lack of serpentine pseudomorphs after anthophyllite, talc, and antigorite in the least-recrystallized samples suggests that olivine and enstatite reacted directly to lizardite pseudomorphs through metastable reactions below 400°C, the highest temperature for the reaction forsterite + water = lizardite + brucite in the MSH system (this estimate is decreased by only 10°C if observed Fe partitionings are used; Moody 1976). This is the common path of serpentinization for most peridotite massifs (Wicks & Whittaker 1977).

The second stage is characterized by the operation of dominantly solid–solid reactions involving the recrystallization of lizardite to form the type-1 hourglass texture, and its replacement by chrysotile + antigorite ± lizardite interlocking texture.

Lizardite was the sole serpentine mineral present in

the Cassiar serpentinite prior to recrystallization, and isochemical recrystallization and replacement should have produced chrysotile, rather than chrysotile + antigorite. The presence of talc–magnetite in the shear zones suggests that the addition of SiO₂ to the serpentinite (or SiO₂ metasomatism) during recrystallization stabilized chrysotile + antigorite.

In the footwall and hanging-wall serpentinites, the presence of relict chromite in several of the proposed reactions, the lack of equilibrium between the lizardite after olivine and that after enstatite in the least-recrystallized serpentinite, and the presence of coexisting textures in many samples all indicate non-equilibrium on a thin-section scale. However, local equilibrium is present because: a) one can formulate a sequence of reactions to describe the changes in mineralogy, composition, and the distribution of the serpentine minerals, and b) the replacement of lizardite by chrysotile + antigorite is the stable assemblage inferred from the phase diagram.

Evaluation of the serpentine –
magnetite thermometer and the stability of chrysotile
+ antigorite in the MSH system

The calculated temperatures and pressures for serpentine recrystallization and replacement overlap the calculated position of the equilibrium chrysotile = antigorite + brucite (Fig. 5). As the textures suggest that antigorite + chrysotile are in equilibrium, and the compositional data suggest that equilibrium was closely approached late in the replacement, we do not believe that the conditions of the above equilibrium were exceeded. This conclusion indicates excellent agreement between the isotope thermometer and the phase-equilibrium data. However, hypothetically, partitioning of Fe into chrysotile, antigorite, and brucite could affect the P–T coordinates of the equilibrium by altering the molar entropies and volumes. Thus it is necessary to evaluate whether the agreement is real or fortuitous.

The above agreement can be explained in one of three ways. One possibility is that the calculated phase-diagram is incorrect. An earlier estimate for the location of the equilibrium chrysotile = antigorite + brucite placed it at 300°C at very low pressures (Evans *et al.* 1976). Solid–solid equilibria are known to be kinetically sluggish, so that it is difficult to obtain phase-equilibrium data for them, especially at low temperatures. In fact, in their review of serpentine phase-equilibria, Chernosky *et al.* (1988) included a reversal of the above equilibrium as one of the critical pieces of information needed to refine the phase diagram. Thus, the location of this equilibrium is not well constrained, and the stability field for chrysotile + antigorite implied by the isotope temperatures would still be consistent with the calculated phase-diagram if the above equilibrium were to be shifted to higher temperatures.

The thermodynamic dataset is a self-consistent one, and models the serpentine-dehydration equilibria well (Berman *et al.* 1986). Therefore, a second possibility is that the calculated phase-diagram is correct and that the temperatures calculated using the serpentine–magnetite thermometer are not correct. The serpentine–magnetite thermometer is an empirical one based on a comparison of serpentine in serpentinite to chlorite in pelitic schists (Wenner & Taylor 1971). Savin & Lee (1988) proposed another curve for serpentine–water fractionation using an empirical calculation based on the type of bonds present. This curve yields similar fractionations to those of Wenner & Taylor (1971) between 250 and 350°C, which is the temperature range of interest. Therefore, although both curves are empirical, they are consistent in the temperature range of interest. Thus there are no other reasons to doubt the thermometer.

A third possibility is that limited incorporation of Fe^{3+} into lizardite and chrysotile is sufficient to alter the P–T coordinates of the solid–solid reactions. For example, greater solubility of Fe^{3+} in chrysotile than in antigorite would change the univariant MSH equilibrium chrysotile = antigorite + brucite to the univariant $Fe^{3+}Fe^{2+}$MSH equilibrium chrysotile = antigorite + brucite + magnetite. Fe^{3+} could stabilize chrysotile to higher temperatures at the expense of antigorite, possibly permitting the stable coexistence of Fe^{3+}-bearing chrysotile + antigorite at temperatures above 300°C. However, as mentioned earlier, we do not believe that the observed partitions are sufficient to significantly alter molar entropies and volumes. Of the three possibilities considered, we contend that the agreement between the temperature estimates obtained from phase equilibria and from stable-isotope fractionations is not fortuitous.

Cause of recrystallization in the ore zone

Recrystallization in the ore zone culminates with a lizardite ± antigorite ± chrysotile ± chlorite ± magnetite ± heazlewoodite assemblage at T = 250 ± 25°C, and $P(H_2O)$ <1 kbar. It is clear, on the basis of evidence presented above, that recrystallization and replacement within the serpentinite increase from both the footwall and the hanging-wall serpentinites into the ore zone, which is spatially related to the 45° and 70° shears. We eliminate classical thermally driven metamorphism as the cause of recrystallization for three reasons. First, the serpentinite is chemically homogeneous (Table 1), so that there is no significant change in bulk composition to justify thermally driven recrystallization of the middle portion of the serpentinite but not its margins. Second, there is no igneous intrusive body centered under the middle of the serpentinite to act as a heat source (nor did exploratory drilling encounter one). Third, thermal metamorphism cannot account for the talc–magnetite assemblage in the 45° shear, which requires a change in bulk-rock composition from that of the serpentinite precursor.

Despite the elimination of thermally driven metamorphism as a cause of recrystallization, heat is needed to produce recrystallization and replacement because the solid–solid reactions are endothermic. However, the enthalpy changes for the solid–solid reactions are small (*e.g.*, 17 kJ/mol for the equilibrium chrysotile = antigorite + brucite; O'Hanley 1991); the reactions did not go to completion, so that not much heat was needed.

An alternative cause of recrystallization is infil-tration-driven metamorphism (Ferry 1989). In this process, a fluid that is thermally or chemically (or both) out of equilibrium with the rock produces recrystalliza-tion as the rock equilibrates with the fluid. Infiltration-driven metamorphism explains the textural patterns, the changes in mineralogy and mineral composition, and explains why the recrystallization is centered about the 45° and 70° shear zones in the middle of the

serpentinite. The presence of an externally derived fluid also accounts for changes in bulk-rock $\delta^{18}O$ values (O'Hanley et al. 1989b) and for consistent changes in bulk-rock compositions during recrystallization of both rodingite and serpentinite (O'Hanley et al. 1992). The shear zones in the middle of the serpentinite were the conduits through which a fluid chemically different (higher activity of SiO_2) from (and perhaps hotter than) the serpentinite, gained access to the serpentinite.

The water/rock value calculated from mineral assemblages using progress of the reaction is the critical parameter used to determine that infiltration-driven metamorphism was the cause of recrystallization (Ferry 1989). Unfortunately, we cannot carry out such a calculation because water is neither consumed nor produced in the solid–solid reactions of hydrated solids, so that the water/rock value is moot to the determination of whether or not infiltration metamorphism occurred at Cassiar. Furthermore, we do not know the initial $\delta^{18}O$ value of the fluid involved in serpentine recrystallization, so that we cannot use the $\delta^{18}O$ values of the different textures to calculate the water/rock value. We also lack measured thermodynamic data for lizardite, and this precludes calculation of a thermal budget. Despite these limitations, there is a great deal of evidence that supports infiltration-driven metamorphism. Also, the elimination of thermally driven metamorphism leaves infiltration-driven metamorphism as the preferred process to account for the development of the ore zone at Cassiar.

Cause of recrystallization in the hanging-wall zone of alteration

The formation of antigorite in the hanging-wall zone of alteration was caused by metasomatic alteration involving rocks of very different compositions: the argillites and greenstones, and the serpentinite. This process produced successive zones, moving from the serpentinites to the wallrocks, of antigorite, tremolite, and tremolite + clinozoisite + quartz (Gabrielse 1963). There are no asbestos veins near this zone, so that deformation was not important. The driving force for recrystallization presumably involved the chemical differences between the two protoliths, and not infiltration-driven metamorphism as envisioned to explain textures in the ore zone. This process appears to have occurred early in the serpentinization history and welded the serpentinite to the hanging-wall rocks. This welding probably focussed successive faulting along the 45° and 70° shears.

CONCLUSIONS

The minerals and textures found in the Cassiar serpentinite are not randomly distributed, but occur in specific patterns with respect to the shear zones. These patterns indicate the sequential development of the various serpentine minerals and textures, and thus the relationships of one to the other. No evidence of the initial hydration of the peridotite is preserved, but some lines of evidence for its presence can be inferred. Recrystallization and replacement of serpentine were complex, but ultimately resulted in the production of antigorite + chrysotile from lizardite. Chemical changes accompanying recrystallization at 250 ± 25°C, <1 kbar indicate that local equilibrium is attained, and equilibrium was approached at the thin-section scale near the 45° and 70° shear zones. The observed mineral assemblages and mineral compositions are consistent with P–T estimates from the MSH model for the serpentine phase-diagram. However, Fe^{3+} may have an important role in promoting isothermal changes among lizardite, chrysotile, and antigorite.

REFERENCES

BERMAN, R.G. (1988): Internally consistent thermodynamic data for minerals in the system $Na_2O–K_2O–CaO–MgO–FeO–Fe_2O_3–Al_2O_3–SiO_2–TiO_2–H_2O–CO_2$. *J. Petrol.* **29**, 445-522.

————, ENGI, M., GREENWOOD, H.J. & BROWN, T.H. (1986): Derivation of internally-consistent thermodynamic data by the technique of mathematical programming: a review with application to the system $MgO–SiO_2–H_2O$. *J. Petrol.* **27**, 1331-1364.

CARPENTER, B.S. (1972): Determination of trace concentration of boron and uranium in glass by the nuclear track technique. *Anal. Chem.* **44**, 600-602.

CARUSO, L.J. & CHERNOSKY, J.V., JR. (1979): The stability of lizardite. *Can. Mineral.* **17**, 757-769.

CHERNOSKY, J.V., JR., BERMAN, R.G. & BRYNDZIA, L.T. (1988): Stability, phase relations, and thermodynamic properties of chlorite and serpentine group minerals. *In* Hydrous Phyllosilicates (Exclusive of Micas) (S.W. Bailey, ed.). *Rev. Mineral.* **19**, 295-346.

CLAYTON, R.N., O'NEIL, J.R. & MAYEDA, T.K. (1972): Oxygen isotope exchange between quartz and water. *J. Geophys. Res.* **77**, 3057-3067.

COLEMAN, R.G. & KEITH, T.E. (1971): A chemical study of serpentinization – Burro mountain, California. *J. Petrol.* **12**, 311-328.

DUNGAN, M.A. (1979): Bastite pseudomorphs after orthopyroxene, clinopyroxene and tremolite. *Can. Mineral.* **17**, 729-740.

EVANS, B.W., JOHANNES, W., OTERDOOM, H. & TROMMSDORFF, V. (1976): Stability of chrysotile and antigorite in the serpentinite multisystem. *Schweiz. Mineral. Petrogr. Mitt.* **56**, 79-93.

FERRY, J.M. (1989): Infiltration-driven metamorphism in northern New England, U.S.A. *J. Petrol.* **29**, 1121-1159.

GABRIELSE, H. (1960): The genesis of chrysotile asbestos in the Cassiar asbestos deposit, northern British Columbia. *Econ. Geol.* **55**, 327-337.

————— (1963): McDame map area, Cassiar District, British Columbia. *Geol. Surv. Can., Mem.* **319**.

————— (1985): Major dextral transcurrent displacements along the northern Rocky Mountain Trench, and related lineaments in north-central British Columbia. *Geol. Soc. Am., Bull.* **96**, 1-14.

HARMS, T. (1986): *Structural and Tectonic Analysis of the Sylvester Allochthon, Northern British Columbia: Implications for Paleogeography and Accretion.* Ph.D. thesis, Univ. of Arizona, Phoenix, Arizona.

HIGGINS, M.D., TRUSCOTT, M.G., SHAW, D.M., BERGERON, M., BUFFET, G.H., COPLEY, J.R.D. & PRESTRICH, W.V. (1984): Prompt gamma neutron activation analysis at McMaster nuclear reactor. *In* Development of Low and Medium Flux Reactors (O.K. Harling, L. Clark & P. van der Hardt, eds.). *Atomkerenergie Kerntechnik* **44**, 690-697.

HOSTETLER, P.B., COLEMAN, R.G., MUMPTON, F.A. & EVANS, B.W. (1966): Brucite in alpine-type serpentinites. *Am. Mineral.* **51**, 75-98.

LAURENT, R. (1980): Regimes of serpentinization and rodingitization in Québec Appalachian ophiolites. *Arch. Sci. Genève* **33**, 311-320.

MERCIER, J.-C.C. & NICOLAS, A. (1975): Textures and fabrics of upper-mantle peridotites as illustrated by xenoliths from basalts. *J. Petrol.* **16**, 454-487.

MOODY, J.B. (1976): An experimental study on the serpentinization of iron-bearing olivines. *Can. Mineral.* **14**, 462-478.

NELSON, J.L. & BRADFORD, J.A. (1993): Geology of the Midway-Casiar area, northern British Columbia (104O, 104P). *B.C. Ministry Energy, Mines, Petrol. Resources, Geol. Surv. Branch, Bull.* **83**.

O'HANLEY, D.S. (1987): A chemographic analysis of magnesian serpentinites using dual networks. *Can. Mineral.* **25**, 121-133.

————— (1988): The origin of alpine peridotite-hosted, cross fiber, chrysotile asbestos deposits. *Econ. Geol.* **83**, 256-265.

————— (1990): The structural geology of the Mount McDame area, north-central British Columbia (104/P). *B.C. Ministry Energy, Mines & Petrol. Resources, Geol. Fieldwork, Pap.* **1990-1**, 223-228.

————— (1991): Fault-related phenomena associated with hydration and serpentine recrystallization during serpentinization. *Can. Mineral.* **29**, 21-35.

—————, CHERNOSKY, J.V., JR. & WICKS, F.J. (1989a): The stability of lizardite and chrysotile. *Can. Mineral.* **27**, 483-493.

————— & DYAR, M.D. (1993): The composition of lizardite 1T and the formation of magnetite in serpentinites. *Am. Mineral.* **78**, 391-404.

—————, KYSER, T.K. & WICKS, F.J. (1989b): Evidence from lizardite/chrysotile serpentinites for proton exchange without recrystallization. *Geol. Soc. Am., Abstr. Programs* **21**(6), A12.

————— & OFFLER, R. (1992): Characterization of multiple serpentinization, Woodsreef, New South Wales. *Can. Mineral.* **30**, 1113-1126.

—————, SCHANDL, E.S. & WICKS, F.J. (1992): The origin of rodingites from Cassiar, British Columbia, and their use to estimate T and P(H₂O) during serpentinization. *Geochim. Cosmochim. Acta* **56**, 97-108.

————— & WICKS, F.J. (1987): Structural control of serpentine textures in the Cassiar Mining Corporation's open-pit mine at Cassiar, British Columbia. *Geol. Assoc. Can. – Mineral. Assoc. Can., Program Abstr.* **12**, 77.

PRICHARD, H.M. (1979): A petrographic study of the processes of serpentinization in ophiolites and the ocean crust. *Contrib. Mineral. Petrol.* **68**, 231-241.

SAVIN, S.M. & LEE, M. (1988): Isotopic studies of phyllosilicates. *In* Hydrous Phyllosilicates (Exclusive of Micas) (S.W. Bailey, ed.). *Rev. Mineral.* **19**, 189-223.

SHIGA, Y. (1987): Behavior of iron, nickel, cobalt and sulfur during serpentinization, with reference to the Hayachine ultramafic rocks of the Kamaishi mining district, northeastern Japan. *Can. Mineral.* **25**, 611-624.

UEHARA, S. & SHIROZU, H. (1985): Variations in chemical composition and structural properties of antigorites. *Mineral. J.* **12**, 299-318.

WENNER, D.B. & TAYLOR, H.P., JR. (1971): Temperatures of serpentinization of ultramafic rocks based on O^{18}/O^{16} fractionation between coexisting serpentine and magnetite. *Contrib. Mineral. Petrol.* **32**, 165-185.

WHITTAKER, E.J.W. & ZUSSMAN, J. (1956): The characterization of serpentine minerals by X-ray diffraction. *Mineral. Mag.* **31**, 107-126.

WICKS, F.J. (1984): Deformation histories as recorded by serpentinites. I. Deformation prior to serpentinization. *Can. Mineral.* **22**, 185-195.

_____ & O'HANLEY, D.S. (1988): Serpentine minerals: structure and petrology. *In* Hydrous Phyllosilicates (Exclusive of Micas) (S.W. Bailey, ed.). *Rev. Mineral.* **19**, 91-167.

_____ & PLANT, G. (1979): Electron microprobe and X-ray microbeam studies of serpentinite textures. *Can. Mineral.* **17**, 785-830.

_____ & WHITTAKER, E.J.W. (1977): Serpentine textures and serpentinization. *Can. Mineral.* **15**, 459-488.

_____, _____ & ZUSSMAN, J. (1977): An idealized model for serpentine textures after olivine. *Can. Mineral.* **15**, 446-458.

_____ & ZUSSMAN, J. (1975): Microbeam X-ray diffraction patterns of the serpentine minerals. *Can. Mineral.* **13**, 244-258.